N O T I C E

THIS DOCUMENT HAS BEEN REPRODUCED FROM MICROFICHE. ALTHOUGH IT IS RECOGNIZED THAT CERTAIN PORTIONS ARE ILLEGIBLE, IT IS BEING RELEASED IN THE INTEREST OF MAKING AVAILABLE AS MUCH INFORMATION AS POSSIBLE

NASA Technical Memorandum 87176

Determination of Convective Diffusion Heat/Mass Transfer Rates to Burner Rig Test Targets Comparable in Size to Cross-Stream Jet Diameter

Süleyman A. Gökoğlu
Case Western Reserve University
Cleveland, Ohio

and

Gilbert J. Santoro
Lewis Research Center
Cleveland, Ohio

DEC 1985
RECEIVED
NASA STI FACILITY
ACCESS DEPT.

(NASA-TM-87176) DETERMINATION OF CONVECTIVE DIFFUSION HEAT/MASS TRANSFER RATES TO BURNER RIG TEST TARGETS COMPARABLE IN SIZE TO CROSS-STREAM JET DIAMETER (NASA) 15 p HC A02/MF A01 CSCL 20D G3/34 N86-13678 Unclas 04972

Prepared for the
31st International Gas Turbine Conference
sponsored by the American Society of Mechanical Engineers
Dusseldorf, Germany, June 8-12, 1986

NASA

DETERMINATION OF CONVECTIVE DIFFUSION HEAT/MASS TRANSFER RATES TO BURNER RIG TEST TARGETS COMPARABLE IN SIZE TO CROSS-STREAM JET DIAMETER

Süleyman A. Gökoğlu* and Gilbert J. Santoro
National Aeronautics and Space Administration
Lewis Research Center
Cleveland, Ohio 44135

ABSTRACT

Two sets of experiments have been performed to be able to predict the convective diffusion heat/mass transfer rates to a cylindrical target whose height and diameter are comparable to, but less than, the diameter of the circular cross-stream jet, thereby simulating the same geometric configuration as a typical burner rig test specimen located in the cross-stream of the combustor exit nozzle. The first set exploits the napnthalene sublimation technique to determine the heat/mass transfer coefficient under isothermal conditions for various flow rates (Reynolds numbers). The second set, conducted at various combustion temperatures and Reynolds numbers, utilizes the temperature variation along the surface of the above-mentioned target under steady-state conditions to estimate the effect of cooling (dilution) due to the entrainment of stagnant room temperature air. The experimental information obtained is used to predict high temperature, high velocity corrosive salt vapor deposition rates in burner rigs on collectors that are geometrically the same. The agreement with preliminary data obtained from Na_2SO_4 vapor deposition experiments is found to be excellent.

NOMENCLATURE

A	area
d	diameter
D	(Fick) diffusion coefficient
DC	discharge coefficient
F(turb)	function describing mainstream turbulence
J"	mass (deposition) flux
L	characteristic length (diameter of cylindrical collector)
$\dot{m}$	mass flowrate (ρUA)
M	molecular weight of gas
Ma	Mach number, U_∞/U_{sonic}
n	exponent of Schmidt number
Nu	mass transfer Nusselt (Sherwood) number
Nu_θ	local (θ-dependent) Nusselt number
p	pressure
R	universal gas constant
Re	Reynolds number
Sc	Schmidt number, $\mu/(\rho D)$
T	absolute temperature
U	velocity
γ	ratio of heat capacity at constant pressure to heat capacity at constant volume
Δ	difference operator
θ	angle from the windward stagnation point
μ	dynamic viscosity of gas
ρ	density of gas
ω	mass fraction of transported species

Subscripts

amb	ambient conditions

*Case Western Reserve University, Department of Mechanical and Aerospace Engineering, Cleveland, Ohio 44106 and NASA Resident Research Associate.

e local outer edge of boundary layer around the collector

eff effective

l leeward stagnation point

lam laminar mainstream

o windward stagnation point

w at the surface (wall)

∞ upstream infinity

Miscellaneous

— averaged quantity

( ) function of argument inside parenthesis

1. INTRODUCTION

Trace amounts of impurities in hot gas flow systems can lead to the deposition of corrosive salts (i.e., sodium sulfate) on cold surfaces, severely deteriorating system performance. The objective of the "hot" corrosion research at NASA Lewis Research Center is to predict hot section component life, specifically for combustion turbine engine applications. For this purpose less expensive (cf. full scale engine testing) high velocity-high temperature (and high pressure) burner rigs, nominally operating at Mach 0.3, were built to measure deposition rates of sodium sulfate on inert, internally cooled, cylindrical collectors located in the cross-stream of Na-salt-doped combustion gases. The purpose of internal cooling (by air impingement) was to independently control the collector surface temperature irrespective of combustion gas and prevailing dew point temperatures. The results of the previous work were reported in detail in Refs. 1 and 2.

The corrosive deposits are formed primarily by the vapor transport of precursors (e.g., NaOH, Na, Na_2SO_4, etc. in the case of Na_2SO_4 deposition) across the boundary layer. A comprehensive, chemically frozen boundary layer vapor transport theory has been recently formulated to predict deposition rates (3,4). However, the complicated aerodynamic conditions prevailing in the burner rig deposition tests necessitated further experimentally determined parameters to be provided to the theory to gain predictive capabilities.

Because of the internal air cooling feature, the collector diameter had to be relatively large with respect to the burner nozzle throat diameter. The collector diameter was 1.91 cm (with a wall thickness of 0.32 cm) and the throat diameter was 2.54 cm. This dimensional relationship facilitates ambient air entrainment and penetration into the hot gases around the collector, causing significant cooling of the mainstream and dilution of precursor contaminants. The full utilization of the extensive literature on both cylinders in crossflow (5-8) and impinging jets (9,10) was limited by the geometric constraints as shown in Fig. 1. Therefore, experiments were performed to determine (a) the discharge coefficient of the burner exit nozzle by exploiting isentropic jet expansions, (b) the mass transfer coefficient and the mainstream turbulence effect (11-16) pertaining to the burner rig test configuration by exploiting the naphthalene sublimation technique (17-19), and (c) the entrained ambient air cooling and dilution effect by exploiting the effective jet impingement cooling concepts (20-23). Predicted sodium sulfate mass transfer (deposition) rates using this information were compared to the preliminary experimental data, and excellent agreement was obtained.

The following analysis is concerned mainly with the effect of the larger diameter rather than the height (1.27 cm) of the cylindrical collector, although the naphthalene sublimation experiments to determine the mass transfer coefficient exactly duplicated the collector geometry.

2. PROBLEM DEFINITION AND APPROACH

For a cylindrical collector in crossflow with the nomenclature given in Fig. 2, the local mass transfer (deposition) flux of a trace ($\omega_\infty << 1$, 1-10 ppm Na in our case) species at the surface can be given by:

$$j_w'' = \frac{\rho_e D_e}{L} \cdot Nu_e \cdot (\omega_e - \omega_w) \qquad (1)$$

In Eq. (1) we deliberately neglected the thermal diffusion (Soret) effect for simplicity although we do include it for our rigorous predictions (3,4). The surface mass fraction of the species, ω_w, is derived from surface reaction (or "sticking") rate constants or equilibrium vapor pressures prevailing at the surface temperature. However, again for the sake of simplicity, although with no loss of generality, we will also assume that $\omega_w << \omega_e$ in our discussions below.

In an ideal cylinder in crossflow situation the collector would be small enough to be totally immersed in the combustion gases such that the angular mass fraction of the dopant species in the mainstream around around the collector, ω_e, would be constant and equal to that in the burner exit gases, ω_∞. Similarly, the mainstream total temperature, T_e, would be the same as the total jet temperature, T_0, of the approach stream. The fact that our collector diameter is comparable to, but less than, the jet diameter, causing the efficient entrainment of ambient air, gives rise to a highly nonadiabatic flow and a nonuniform concentration mainstream. In turn, the local thermodynamic and transport properties become angle dependent. Moreover, the entrainment and mixing taking place in the mainstream may be strong enough to influence the boundary layer aerodynamic structure to, eventually, cause the mass transfer Nusselt (Sherwood) number, Nu_e, to have an angle dependence other than its customary cubical relationship (24) obtained in "perfect" cylinder in crossflow studies. Therefore, the average deposition flux on the collector is given by:

$$\overline{j_w''} = \frac{1}{2\pi L} \int_0^{2\pi} \rho_e(T_e(\theta)) \cdot D_e(T_e(\theta)) \cdot Nu_e(\theta, T_e(\theta)) \cdot \omega_e(\theta) \cdot d\theta \equiv \frac{1}{L} \cdot \overline{(\rho_e D_e Nu_e \omega_e)} \qquad (2)$$

Note that the perimeter averaged product is not the same as the product of the individual perimeter averaged quantities. Therefore, an approach directed at obtaining the isolated effective mainstream concentration, $\overline{\omega}_e$ ($\approx \overline{\omega_e - \omega_w}$), and the isolated effective Nusselt number, $\overline{Nu}_e$, etc. via properly designed experiments and then taking their product would not give the correct total deposition rate. Cognizant of the difficulty involved in determining the angular variation of the local, ω_e, T_e and Nu_e, we have taken a

path that would give a reasonable engineering prediction of total deposition rates on our collectors, minimizing the error within the constraints of our experimental facilities.

2.a. The Discharge Coefficient of the Burner Exit Nozzle

For our burner rig test conditions at flame temperatures of 1500 to 2000 K and at Mach numbers of about 0.3, the Reynolds number range of interest is determined to be between 1.5 to 2.0×10^4. Experiments under equivalent aerodynamic conditions require carefully determined Reynolds numbers which depend on jet approach velocities, U_∞. For the correct calculation of U_∞, therefore, first the discharge coefficient of the burner exit nozzle was experimentally determined as a function of Reynolds number by measuring the stagnation pressure of the jet stream at ambient temperature for known mass flow rates of air.

2.b. The F{turb} Factor and the Mass Transfer Nusselt Number

In Eqs. (1) and (2), Nu_e actually includes the effect of mainstream turbulence effect on convective diffusion mass transport; i.e., it can be expressed as,

$$Nu_e = F\{turb\}\, Nu_{e,lam} \qquad (3)$$

where $Nu_{e,lam}$ is the Nusselt number for the laminar mainstream and the effect of mainstream turbulence is factored out as $F\{turb\}$. Stagnation point region naphthalene sublimation experiments (25) for which $Nu_{o,lam}$ can be theoretically calculated were used to determine $F\{turb\}$ at various Reynolds numbers.

For the Reynolds number range of our interest about 65 percent of the total deposit is collected on the windward surface ($-\pi/2 \leq \theta \leq \pi/2$) of ideal cylinders in crossflow (26). In our situation, because the leeward ($\pi/2 \leq \theta \leq 3\pi/2$) mainstream concentration of the species is less than the windward concentration due to dilution, even a higher percentage of the total deposit will be collected on the windward surface of our collectors. Therefore, we divide our analysis into two parts (a) the windward section: the primary region which is treated more rigorously by more direct experimental information, and (b) the leeward section: the secondary region for which some justifiable rational estimations were made. Geometric symmetry allows us below to only deal with angles for which $0 \leq \theta \leq \pi$.

For the windward section, after determining that for the Re range of interest $F\{turb\}$ is unity, we experimentally verified the traditional Nusselt number angular dependence, i.e.,

$$Nu_e(\theta) = Nu_o \left\{ 1 - \left[\frac{\theta}{(\pi/2)} \right]^3 \right\}, \qquad 0 \leq \theta \leq \frac{\pi}{2} \qquad (4)$$

by using the naphthalene sublimation technique and by exposing different angular fractions ($\theta = \pi/9, \pi/6, \pi/4, \pi/3$) of the naphthalene cast cylinders of the same dimensions as collectors. The details of the experimental technique and procedure are given in Ref. 25.

For the leeward section, the angular dependence of the Nusselt number is obtained via an indirect approach. Because exposing certain angular fractions of the naphthalene surface is technically more difficult and subject to greater experimental error, we did full cylinder naphthalene sublimation experiments to determine the perimeter averaged Nusselt number, Nu. For the Re range of interest, the full cylinder experimental data agreed perfectly with the Whitaker correlation (27) indicating that the boundary layer aerodynamic structure is not actually affected by mainstream entrainment phenomena, and that correlations for "perfect" cylinders in crossflow to obtain the mass transfer coefficient apply even to cylinders of our dimensions. The leeward section Nu_e angular distribution inferred from the Whitaker correlation gave a leeward stagnation point Nusselt number, Nu_l, which is in very good agreement with the reported literature values (13,28).

Note that the sublimation technique is an essential feature of our approach, as opposed to many other heat or mass deposition techniques, to determine the mass transfer Nusselt number and its angular variation. The reasons are two-fold: (a) the direction of mass transfer (from surface to mainstream) enables us to exploit the zero mainstream mass fraction of the species ($\omega_e = 0$) as one of our boundary condition regardless of the presence of the entrainment phenomenon (mainstream dilution effect), and (b) the experiments were run under ambient conditions such that the entrained ambient air did not affect the mainstream temperature (mainstream cooling effect). Therefore, an isolated study of Nu_e independent of mainstream entrainment consequences was possible.

2.c. The Cooling and Dilution Effects Due to Entrainment

The approach taken to determine the angular variation of the mainstream cooling effect was to measure the angular variation of the surface temperature of collectors made of different materials at different Re's and T_∞'s. Independent of whether the collector was high thermal conductivity platinum-20 percent rhodium or low thermal conductivity alumina ceramic, and irrespective of Re and T_∞ within the burner operation range of interest, when the normalized collector surface temperature, $(T\{\theta\} - T_l)/(T_o - T_l)$, was plotted against angle, a "universal" curve emerged. We then assumed that the mainstream had the same normalized temperature distribution and derived the mainstream $T\{\theta\}$ after measuring the hot gas temperatures for T_o and T_l.

Because the collector thickness was small compared with its diameter, heat conduction is basically along the circumference (one-dimensional). The Biot numbers calculated for the metallic Pt-20 percent Rh collectors were typically around 0.5 (and larger for ceramic collectors). Since ΔT's between the gas windward and leeward stagnation temperatures were typically around 850 K, we were able to measure ΔT's around 250 K between the metallic collector windward and leeward stagnation temperatures (and larger for ceramic collectors).

In our analysis the mainstream temperature distribution is described by $T\{\theta\}$ for the windward section. However, for the leeward section of secondary importance an effective temperature, $T_{l,eff}$, is used which is obtained from the integral average of the gas temperature distribution over the leeward section. The dilution effect is derived via the heat/mass transfer analogy.

The overall approach described in this section provides the rationale for the evaluation of the integral given by Eq. (2) to predict total collector deposition rates to within reasonable engineering accuracy.

3. IMPLEMENTATION AND RESULTS

3.a. The Discharge Coefficient of the Burner Exit Nozzle

The discharge coefficient of the burner exit nozzle is defined as the ratio of the effective area of the jet nozzle through which gas with a uniform velocity profile passes to the geometric nozzle area, i.e.,

$$DC = \frac{A_{eff}}{A_{nozzle}} \qquad (5)$$

The true jet exit velocity at ambient conditions can be obtained from the isentropic jet expansion relationship, i.e.,

$$U_\infty = U_{sonic}\left\{\left[\left(1 + \frac{\Delta p}{p_\infty}\right)^{(\gamma-1)/\gamma} - 1\right]\frac{2}{\gamma - 1}\right\}^{1/2} \qquad (6)$$

where $\Delta p = p_0 - p_\infty$ and $U_{sonic} = (\gamma RT/M)^{1/2}$. However, for a known gas mass flowrate, $\dot{m}$, using the ideal gas law, the effective nozzle area is given by,

$$A_{eff} = \frac{RT_\infty}{p_\infty M}\frac{\dot{m}}{U_\infty} \qquad (7)$$

We, therefore, used air at ambient conditions and measured Δp and p_∞ for each $\dot{m}$. The direct measurement of Δp instead of p_0 greatly reduces the experimental uncertainty involved (cf. Eq. (6)) in determining U_∞. The Reynolds number based on nozzle diameter is then calculated from

$$Re = \frac{(\dot{m}/DC)d_{nozzle}}{\mu} \qquad (8))$$

A plot of DC versus Re is shown in Fig. 3 where the error bars indicate the experimental scatter. Note that equivalent aerodynamic conditions of interest at flame temperatures (the same Re's) is only the lower end of Fig. 3 ($2.0\times10^4 \le Re \le 2.7\times10^4$ where Re is based on the nozzle throat diameter) since we were limited by the lowest possible air mass flowrate at ambient conditions.

3.b. The F{turb} Factor and the Mass Transfer Nusselt Number

The Nusselt number averaged over some windward angle, θ, can be obtained from Eq. (4) as,

$$\overline{Nu}_e = Nu_0\left\{1 - \frac{1}{4}\left[\frac{\theta}{(\pi/2)}\right]^3\right\}, \qquad 0 \le \theta \le \frac{\pi}{2} \qquad (9)$$

where the stagnation point Nusselt number, Nu_0, is given by (29)

$$Nu_0 = F\{turb\}(1.14)Re^{1/2}\,Sc^n \qquad (10)$$

The exponent of the Schmidt number, n, varies between 1/3 and 0.4 in the literature (7,27,29). Our experiments, shown in Fig. 4 and run for Re range of interest (Re = 1.5 to 2.0×10^4) where the angle of exposed naphthalene surface was about $\theta = 5\pi/18$ (~50°), indicate that (a) F{turb} is unity, (b) the cubical relationship in Eqs. (4) and (9) is a satisfactory description of the angle dependence of Nu_e, and (c) experiments are within ±3 percent of the theoretical values (Eq. (9)) if n = 0.35, consistent with the literature values. The details explaining the experimental scatter as well as the calculation of the experimental Nusselt numbers using the naphthalene vapor pressure values reported in the literature (30-33) are given in Ref. 25.

The experimental perimeter averaged mass transfer Nusselt numbers for fully exposed naphthalene cast cylinders were compared to the Whitaker correlation given by,

$$\overline{Nu}_{lam} = \left(0.4\,Re^{1/2} + 0.06\,Re^{2/3}\right)Sc^n \qquad (11)$$

In the Re range of interest, the best agreement is obtained again within ±3 percent if n = 0.38 (F{turb} is unity), also consistent with the literature. The full cylinder naphthalene sublimation experiments at ambient conditions verified the applicability of the Whitaker correlation for cylinders with our dimensions.

Both the segmented (partially exposed) and full cylinder naphthalene sublimation experiments were extended to higher mass flowrates outside the Re range of interest. As shown in Figs. 5 and 6, the quality of data for full cylinders is better at higher Re than segmented cylinders, because full cylinder experiments are more straightforward and do not involve careful covering of the unexposed portion by taping (see details in Ref. 25). In fact, the full cylinder experimental data was so reproducible that the uncertainty was entirely due to the precision of the naphthalene surface temperature measurement, as indicated by the error bars in Fig. 5. The circles and squares in Fig. 5 are actual full cylinder Nusselt numbers experimentally determined as a function of exposure time of naphthalene surface to flow (duration of experiment), showing the linearity of naphthalene weight loss with time. As a part of the characterization of our burner rigs in their full operation range, we also determined the F{turb} factor by taking the ratio of Nusselt numbers determined experimentally to the ones obtained from correlations. As shown in Fig. 7, both segmented and full cylinder data give F{turb} factors that could be described by a single curve within experimental accuracy. (Note again that the scatter of data for segmented cylinders is larger at higher Reynolds numbers.) This observation is a supporting evidence for the fact that F{turb} is angle independent around the cylinder and can be factored out from $Nu_{e,lam}$ for our setup. However, since F{turb} is unity for our interest range, it will be dropped from our treatment below.

A consistency check for the windward section between Eq. (9) obtained from Eq. (4) and the Whitaker correlation (Eq. (11)) for full cylinders shows that for equal Schmidt number exponents, n, the laminar portion (proportional to $Re^{1/2}$) of the Whitaker correlation can indeed be derived from Eq. (9) with the same coefficient, 0.4. The same type of check for the leeward section can be inversely applied to the Whitaker correlation which has an explicit $Re^{2/3}$ term different than the Froessling relation (34) to account for the increasing importance of the wake region. Therefore, if one assumes the same cubical decline relationship as in Eq. (9) for the leeward section of the cylinder corresponding to turbulent separated flow proportional to $Re^{2/3}$ (a reasonable assumption for Re < ~10^5 (35)), the leeward stagnation point Nusselt number, $\overline{Nu}_l$, can be derived from Eq. (11) (again for equal n's) giving

ORIGINAL PAGE IS
OF POOR QUALITY

$$Nu_1 = 0.160\ Re^{2/3}\ Sc^n \tag{12}$$

The coefficient 0.160 is consistent with the correlation of Ref. 28 which proposes 0.171, and the experiments of Ref. 13 which suggest 0.153 as the premultiplier of $Re^{2/3}$. Therefore, based on above analyses which are further supported by our own experiments given in Figs. 4 and 5, we take Eq. (4) for the windward section, and

$$Nu_e(\theta) = Nu_1 \left\{ 1 - [(\pi - \theta)/(\pi/2)]^3 \right\}, \qquad \frac{\pi}{2} \le \theta \le \pi \tag{13}$$

for the leeward section. Note that Eqs. (4) and (13) assume that the flow separates at $\theta = \pi/2$.

3.c. The Cooling and Dilution Effects Due to Entrainment

Angular dependence of the cooling and dilution effect due to entrainment is obtained by the method described in section 2.c. The resulting curve is shown in Fig. 8 which is well fitted by two simple parabolas:

$$\frac{T_e(\theta) - T_{amb}}{T_o - T_{amb}} = \frac{\omega_e(\theta)}{\omega_o} = 1 - 0.33 \left[\frac{\theta}{(\pi/2)}\right]^2, \qquad 0 \le \theta \le \frac{\pi}{2} \tag{14}$$

$$\frac{T_e(\theta) - T_{amb}}{T_o - T_{amb}} = \frac{\omega_e(\theta)}{\omega_o} = \left[1 - \left(\frac{\theta}{\pi}\right)\right]^2 + 0.42, \qquad \frac{\pi}{2} \le \theta \le \pi \tag{15}$$

$T_{1,eff}$ and $\omega_{1,eff}$ derived from Eq. (15) for the leeward section are then given by,

$$T_{1,eff} = 0.50\ (T_o + T_{amb}), \qquad \omega_{1,eff} = 0.50\ \omega_o \tag{16}$$

3.d. Prediction of Deposition Rates

The temperature dependencies of the thermodynamic and transport properties pertaining to air and Na-carrier species (i.e., Na, NaOH, Na_2SO_4, etc.) for the windward section will be described by the simple power laws (24,36)

$$\rho_e(\theta) = \rho_o [T_e(\theta)/T_o]^{-1}, \qquad 0 \le \theta \le \frac{\pi}{2} \tag{17}$$

$$D_e(\theta) = D_o [T_e(\theta)/T_o]^{1.70}, \qquad 0 \le \theta \le \frac{\pi}{2} \tag{18}$$

$$\mu_e(\theta) = \mu_o [T_e(\theta)/T_o]^{0.70}, \qquad 0 \le \theta \le \frac{\pi}{2} \tag{19}$$

Consequently, the Schmidt number becomes temperature independent and for a fixed mass flowrate,

$$Nu_e(T_e(\theta)) = Nu_e(T_o)[T_e(\theta)/T_o]^{-0.35}, \qquad 0 \le \theta \le \frac{\pi}{2} \tag{20}$$

If the local temperature and angular effects for the Nusselt number are mutually exclusive and can be factored out, i.e.,

$$Nu_e(\theta, T_e(\theta)) = Nu_o [T_e(\theta)/T_o]^{-0.35} \left\{ 1 - \left[\frac{\theta}{(\pi/2)}\right]^3 \right\}, \qquad 0 \le \theta \le \frac{\pi}{2} \tag{21}$$

then Eqs. (17), (18), (21), and (14) can be substituted in Eq. (2) to give

$$\bar{j}''_w(\text{windward}) = \frac{j''_o}{(\pi/2)} \int_0^{\pi/2} \left\{ 1 - 0.33 \left[1 - \left(\frac{T_{amb}}{T_o}\right)\right] \left[\frac{\theta}{(\pi/2)}\right]^2 \right\}^{0.35} \times \left\{ 1 - \left[\frac{\theta}{(\pi/2)}\right]^3 \right\} \left\{ 1 - 0.33 \left[\frac{\theta}{(\pi/2)}\right]^2 \right\} d\theta \tag{22}$$

Approximating the bracket with the exponent by the first term of its Taylor series expansion and using the fact that $T_{amb}/T_o \le 0.2$, Eq. (22) can now be easily integrated to obtain the average deposition flux on the windward surface of the collector:

$$\bar{j}''_w(\text{windward}) = (0.68)\ j''_o \tag{23}$$

Because the leeward effective temperature, $T_{1,eff}$, and mass fraction, $\omega_{1,eff}$, are constant, after substituting Eq. (13) into Eq. (2), the average deposition flux for the leeward section is obtained from a straightforward integration of Eq. (2):

$$\bar{j}''_w\ (\text{leeward}) = (0.75)\ j''_1(T_{eff}) = (0.75)\ \frac{\rho(T_{eff})D(T_{eff})}{L}\ Nu_1(T_{eff})\omega_{1,eff} \tag{24}$$

Note that if one assumed no entrainment effect for the windward section and perfect turbulent mixing for the leeward section (i.e., a step function for the temperature distribution given by T_o for the windward and by $T_{1,eff}$ for the leeward section), then Eq. (23) would also read as

$$\bar{j}''_w(\text{windward}) = (0.75)\ j''_o \tag{25}$$

Equations (23) and (24) can now be used for each of the Na-carrier species like Na, NaOH, Na_2SO_4, etc. (multicomponent transport) to calculate the total elemental Na flux to the collector surface which can then be converted into equivalent Na_2SO_4 deposition rates. Because sodium is in trace amounts, sulfur (from jet A-1 fuel) and oxygen (left over after combustion) are excessively available to form sodium sulfate.

3.e. Comparison of Theory and Experiment

For the burner rig deposition experiments Na-acetate dissolved in alcohol is used as the Na source. The Na-acetate/alcohol solution is mixed with jet A-1 fuel in the fuel nozzle cavity and sprayed into the

combustor through the fuel nozzle to assure the complete vaporization and chemical equilibrium of Na-carrier species. However, some of the Na fed into the system deposits on the inner wall of the cool end of the burner liner after the fuel and the alcohol burn away. From chemical analyses we currently estimate that about 25 percent of the total Na added is lost on the liner wall and, therefore, the Na concentration in the burner exit combustion gases is effectively so much less. Direct measurement of Na concentration in the combustion effluent gases will be done in situ by the Na-emission spectrometry technique in the near future. The collector located 5/8 inch from the burner nozzle is rotated with a velocity much smaller than the jet stream velocity to keep the surface temperature constant and uniform.

Predictions made as described above, including also the thermal (Soret) diffusion effect (only about 2 to 3 percent in our case), are compared with the experimental deposition rates as shown in Fig. 9. All the experiments were run under the following conditions: $Ma_\infty = 0.3$, $Re = 1.74 \times 10^4$, fuel to air flowrate ratio = 0.035, $T_0 = 1800$ K. The prediction band refers to 30 percent (lower curve) and 20 percent (higher curve) loss of total Na fed into the system on the burner liner wall (estimated at 25 percent, resulting in a net 5 ppm sodium concentration with respect to the combustion air). Excellent agreement is found between theory and experiment for the plateau region. The disagreement above the melting point of Na_2SO_4 (884 °C) is due to shear driven molten deposit layer run-off from the smooth collector surface (1, 37) resulting in lower experimental values. It should be noted that about 83 percent of the total deposition is predicted to occur on the windward surface of the collector, justifying our original premise that the windward section should be treated more carefully.

The chemical equilibrium calculations for the conditions prevailing in the leeward section ($\omega_{1,eff} = 0.50\ \omega_0 = \sim 2.5$ ppm Na in air, $T_{1,eff} = 0.50\ (T_0 + T_{amb}) = \sim 1050$ K, p = 1 atm) using the NASA CEC code (38) indicate that the gas stream is supersaturated (supersaturation ratio = 9×10^2) and Na_2SO_4 particles should condense. If the homogeneous kinetics is indeed fast enough for nucleation (based on the estimates given in Ref. 3, the critical supersaturation ratio is expected to be larger than 10^3 for these conditions), then the submicron particles formed would be transported by thermophoresis (39-41). However, since the gas stream is cool in the leeward section and the gas stream to collector surface temperature contrast, T_w/T_e, is not sufficient, one would hardly expect any deposition on the leeward surface by thermophoresis.

A simple experiment was designed to check if there was any mainstream condensation. For that purpose an inert segmented collector 20° on each side of the leeward stagnation point (the rest of the cylinder being made of silicon nitride ceramic) is used to measure leeward stagnation point region deposition rates. Deposition was indeed observed on the segmented collector and the measured rates agreed well with what was expected from multicomponent vapor deposition rates described above, indicating that no condensation took place in the gas stream. It should be noted that even if condensation had taken place, our predicted deposition rate would have been in error by a maximum of 20 percent.

4. CONCLUSIONS

Convective diffusion mass transfer (deposition) rates to cylindrical burner rig test targets comparable in size to cross-stream jet diameter have been determined. The naphthalene sublimation technique under isothermal conditions has been utilized for both full and segmented (partially exposed) cylinders of the same dimensions as burner rig collectors to obtain the angular variation of the mass transfer coefficient on the windward and leeward surfaces. Because the relatively large size of the collector causes the ambient air to be entrained, cooling and diluting the mainstream around the collector, the angular variation of the concentration of precursor species and temperature has also been determined.

Information available in the literature on heat and mass transport for cylinders in cross flow and impinging jets has been extensively exploited. The previously developed chemically frozen boundary layer multicomponent vapor deposition theory (3,4) has been adapted for a practical situation to handle corrosive salt deposition rate predictions by making rational assumptions and reasonable engineering approximations with the aid of necessary supplementary experiments. Excellent agreement is obtained between the predicted and experimental sodium sulfate deposition rates on our burner rig collectors within experimental uncertainty.

Although the application is presented for a specific setup in this paper, the extension/generalization of the methodology is certainly possible especially when combined with the study of Ref. 10.

REFERENCES

1. Santoro, G.J.; Kohl, F.J.; Stearns, C.A.; Gokoglu, S.A.; and Rosner, D.E.: Experimental and Theoretical Deposition Rates from Salt-Seeded Combustion Gases of a Mach 0.3 Burner Rig. NASA TP-2225, 1984.

2. Santoro, G.J.; Gökoğlu, S.A.; Kohl, F.J.; Stearns, C.A.; and Rosner, D.E.: Deposition of Na_2SO_4 From Salt-Seeded Combustion Gases of a High Velocity Burner Rig. NASA TM-83751, 1984.

3. Rosner, D.E.; Chen, B.K.; Fryburg, G.C.; and Kohl, F.J.: Chemically Frozen Multicomponent Boundary Layer Theory of Salt and/or Ash Deposition Rates from Combustion Gases. Combust. Sci. Technol., vol. 20, no. 3/4, 1979, pp. 87-106.

4. Gökoğlu, S.A.; Chen, B.K.; and Rosner, D.E.: Computer Program for the Calculation of Multicomponent Convective Diffusion Deposition Rates from Chemically Frozen Boundary Layer Theory. NASA CR-168329, 1984.

5. Zukauskas, A.: Heat Transfer from Tubes in Crossflow. Advances in Heat Transfer, vol. 8, 1972, pp. 93-160.

6. Achenbach, E.: Total and Local Heat Transfer from a Smooth Circular Cylinder in Cross-Flow at High Reynolds Number. Int. J. Heat Mass Transfer, vol. 18, 1975, pp. 1387-1396.

7. Churchill, S.W.; and Bernstein, M.: A Correlating Equation for Forced Convection from Gases and Liquids to a Circular Cylinder in Crossflow. J. Heat Transfer, vol. 99, 1977, pp. 300-306.

8. Peller, H.; Lippig, V.; Straub, D.; and Waibel, R.: Thermofluiddynamic Experiments with a Heated and Rotating Circular Cylinder in Crossflow, Part 1: Subcritical Heat Transfer Measurements. Exp. Fluids, vol. 2, 1984, pp. 113-120.

9. Martin, H.: Heat and Mass Transfer between Impinging Gas Jets and Solid Surfaces. Adv. Heat Transfer, vol. 13, 1977, pp. 1-60.

10. Sparrow, E.M.; and Alnomoud, A.: Impingement Heat Transfer at a Circular Cylinder due to an Offset or Non-Offset Slot Jet. Int. J. Heat Mass Transfer, vol. 27, no. 12, 1984, pp. 2297-2306.

11. Kestin, J.: The Effect of Free-Stream Turbulence on Heat Transfer Rates. Adv. Heat Transfer, vol. 3, 1966, pp. 1-32.

12. Lowery, G.W.; and Vachon, R.I.: The Effect of Turbulence on Heat Transfer from Heated Cylinders. Int. J. Heat Mass Transfer, vol. 18, 1975, pp. 1229-1242.

13. Yardi, N.R.; and Sukhatme, S.P.: Effects of Turbulence Intensity and Integral Length Scale of a Turbulent Free Stream on Forced Convection Heat Transfer from a Circular Cylinder in Cross Flow. International Heat Transfer Conference, 6th, Toronto, Canada vol. 5, 1978, pp. 347-352.

14. Gorla, R.S.R.; and Nemeth, N.: Effects of Free Stream Turbulence Intensity and Integral Length Scale on Heat Transfer from a Circular Cylinder in Crossflow. International Heat Transfer Conference, 7th, Munich, West Germany, 1982, pp. 153-158.

15. Simoneau, R.J.; Morehouse, K.A.; VanFossen, G.J.; and Behning, F.P.: Effect of a Rotor Wake on Heat Transfer from a Circular Cylinder. NASA TM-83613, 1984.

16. Fairweather, M.; Kilham, J.K.; and Mohebi-Ashtiani, A.: Stagnation Point Heat Transfer from Turbulent Methane-Air Flames. Combust. Sci. Technol. vol. 35, 1984, pp. 225-238.

17. Sparrow, E.M.; Stahl, T.J.; and Traub, P.: Heat Transfer Adjacent to the Attached End of a Cylinder in Crossflow. Int. J. Heat Mass Transfer, vol. 27, no. 2, 1984, pp. 233-242.

18. Marziale, M.L.; and Mayle, R.E.: Effect of an Oscillating Flow Direction on Leading Edge Heat Transfer. J. Eng. Gas Turbines Power, vol. 106 1984, pp. 222-228.

19. Goldstein, R.J.; and Karni, J.: The Effect of a Wall Boundary Layer on Local Mass Transfer From a Cylinder in a Crossflow. J. Heat Transfer, vol. 106, 1984, pp. 260-267.

20. Striegl, S.A.; and Diller, T.E.: The Effect of Entrainment Temperature on Jet Impingement Heat Transfer. J. Heat Transfer, vol. 106, 1984 pp. 27-33.

21. Hollworth, B.R.; and Gero, L.R.: Entrainment Effects on Impingement Heat Transfer. Part II: Local Transfer Measurements. ASME-AIChE 22nd National Heat Transfer Conference Niagara Falls, New York, 1984, ASME Paper No. 84-HT-20.

22. Hollworth, B.R.; and Wilson, S.I.: Entrainment Effects on Impingement Heat Transfer: Part I: Measurements of Heated Jet Velocity and Temperature Distributions and Recovery Temperatures on Target Surface. J. Heat Transfer, vol. 106, 1984, pp. 797-803.

23. Striegl, S.A.; and Diller, T.E.: An Analysis of the Effect of Entrainment Temperature on Jet Impingement Heat Transfer. J. Heat Transfer, vol. 106, 1984, pp. 804-810.

24. Martinelli, R.C.; Guibert, A.G.; Morrin, E.H.; and Boelter, L.M.K.: An Investigation of Aircraft Heaters VIII - A Simplified Method for the Calculation of the Unit Thermal Conductance Over Wings. NACA Wartime Report, ARR WR-W-14, March 1943.

25. Santoro, G.J.; and Gökoğlu, S.A.: Experiments for the Determination of Convective Diffusion Heat/Mass Transfer Rates to Burner Rig Test Targets Comparable in Size to Cross-Stream Jet Diameter. to be presented at the 1986 ASME Winter Annual Meeting, Anaheim, California, November 30-December 5, 1986.

26. Gökoğlu, S.A.; and Rosner, D.E.: Technical Note 'Windward Fraction' of the Total Mass or Heat Transport for Flow Past a Circular Cylinder. Aerosol Sci. Technol., vol. 2, no. 4, 1983, pp. 543-544.

27. Whitaker, S.: Elementary Heat Transfer Analysis, Pergamon Press, (1975).

28. Richardson, P.D.: "Heat and Mass Transfer in Turbulent Separated Flows," Chem. Eng. Sci., vol. 18, 1963, p. 149-155.

29. Kays, W.M.; and Crawford, M.E.: Convective Heat and Mass Transfer, Second ed., McGraw Hill, 1980.

30. Camin, D.L.; and Rossini, F.D.: Physical Properties of Fourteen American Petroleum Institute Research Hydrocarbons, C_9 to C_{15}. J. Phys. Chem. vol. 59, 1955, pp. 1173-1179.

31. Vargaftik, N.B.: Tables on the Thermophysical Properties of Liquids and Gases, Second ed., John Wiley, 1975, p. 359.

32. Soyin, H.H.: Sublimation from Disks to Air Streams Flowing Normal to Their Surfaces. Trans. ASME, vol. 80, 1958, pp. 61-69.

33. Ambrose, D.; Lawrenson, I.J.; and Sprake, C.H.S.: The Vapor Pressure of Naphthalene. J. Chem. Thermodynamics, vol. 7, 1975, pp. 1173-1176.

34. Froessling, N.: Evaporation, Heat Transfer, and Velocity Distribution in Two-Dimensional and Rotationally Symmetrical Laminar Boundary-Layer Flow. NACA TM-1432, 1958.

35. Giedt, W.H.: Principles of Engineering Heat Transfer, D. Van Nostrand Co., 1957.

36. Gökoğlu, S.A.; and Rosner, D.E.: Engineering Correlations of Variable-Property Effects on Laminar Forced Convection Mass Transfer for Dilute Vapor Species and Small Particles in Air. NASA CR-168322, 1984.

37. Rosner, D.E.; Gunes, D.; and Nazin-Anous, N.: Aerodynamically Driven Condensate Layer Thickness Distributions on Isothermal Cylindrical Surfaces. Chem. Eng. Commun., vol. 24, 1983, pp. 275-287.

38. Gordon S.; and McBride, B.J.: Computer Program for Calculation of Complex Chemical Equilibrium Compositions, Rocket Performance, Incident and Reflected Shocks, and Chapman-Jouget Detonations. NASA SP-273, 1971.

39. Gökoğlu, S.A.; and Rosner, D.E.: Correlation of Thermophoretically-Modified Small Particle Diffusional Deposition Rates in Forced Convection Systems with Variable Properties, Transpiration Cooling and/or Viscous Dissipation. Int. J. Heat Mass Transfer, vol. 27, no. 5, 1984, pp. 639-645.

40. Gökoğlu, S.A.; and Rosner, D.E.: Thermophoretically-Enhanced Mass Transport Rates to Solid and Transpiration-Cooled Walls Across Turbulent (Law-of-the-Wall) Boundary Layers. Ind. Eng. Chem. Fundam., vol. 24, no. 2, 1985, pp. 208-214.

41. Gökoğlu, S.A.; and Rosner, D.E.: Thermophoretically-Augmented Forced Convection Mass Transfer Rates to Solid Walls Across Non-Isothermal Laminar Boundary Layers. AIAA J., vol. 24, (January 1986).

ORIGINAL PAGE IS
OF POOR QUALITY

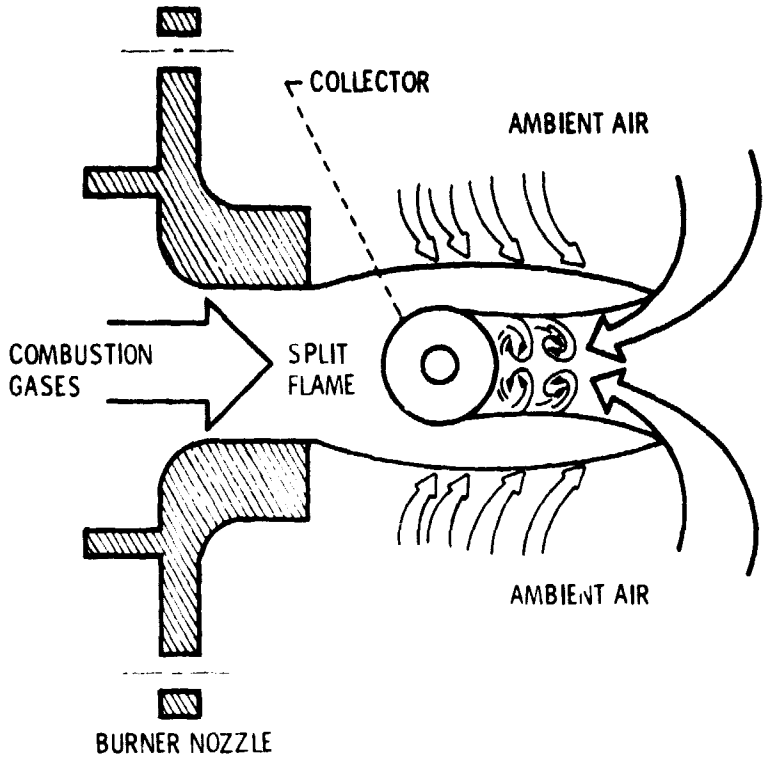

Figure 1. - Schematic of burner rig and collector configuration showing ambient air entrainment.

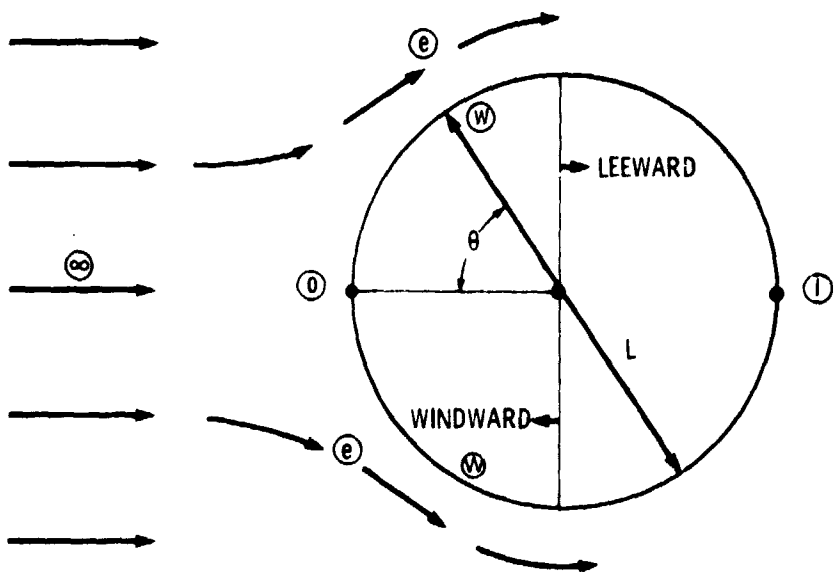

Figure 2. - Station nomenclature for the cylindrical collector.

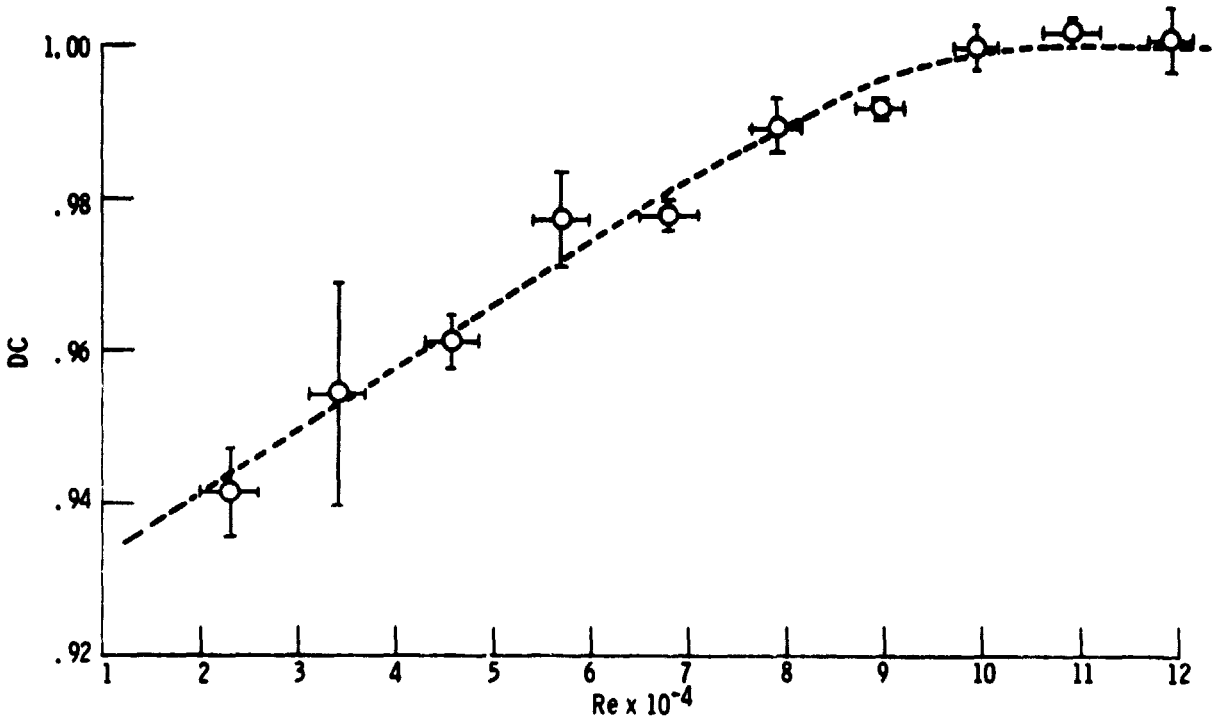

Figure 3. - Burner exit nozzle discharge coefficient as a function of Reynolds number based on nozzle diameter.

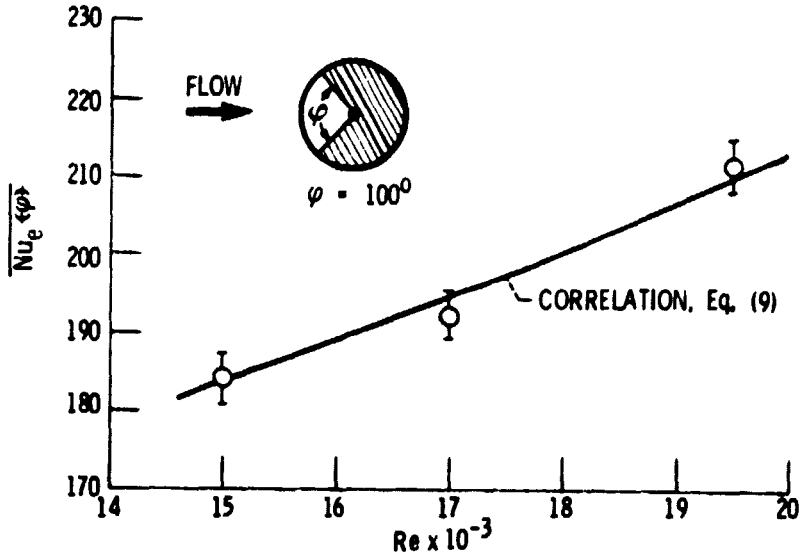

Figure 4. - Stagnation point region mass transfer Nusset number obtained by the naphthalene sublimation technique as a function of Reynolds number (based on collector diameter) for the range of interest.

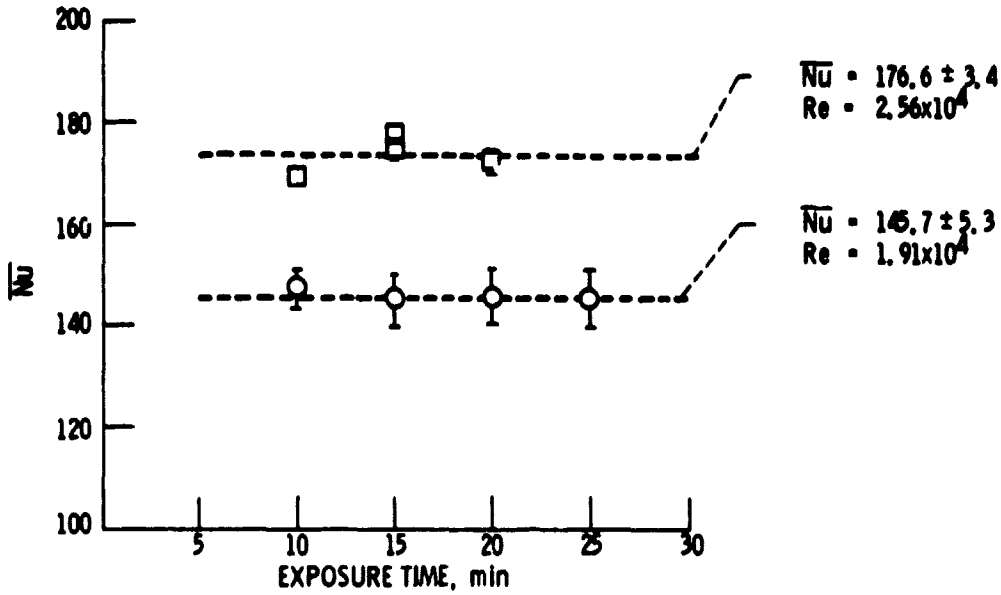

Figure 5. - Full cylinder mass transfer Nusselt number obtained by the naphthalene sublimation technique as a function of time of exposure to flow (duration of experiment) showing linearity of naphthalene weight loss. The circles and squares are reproducable experimental values; error bars indicate uncertainty in naphthalene surface temperature measurement.

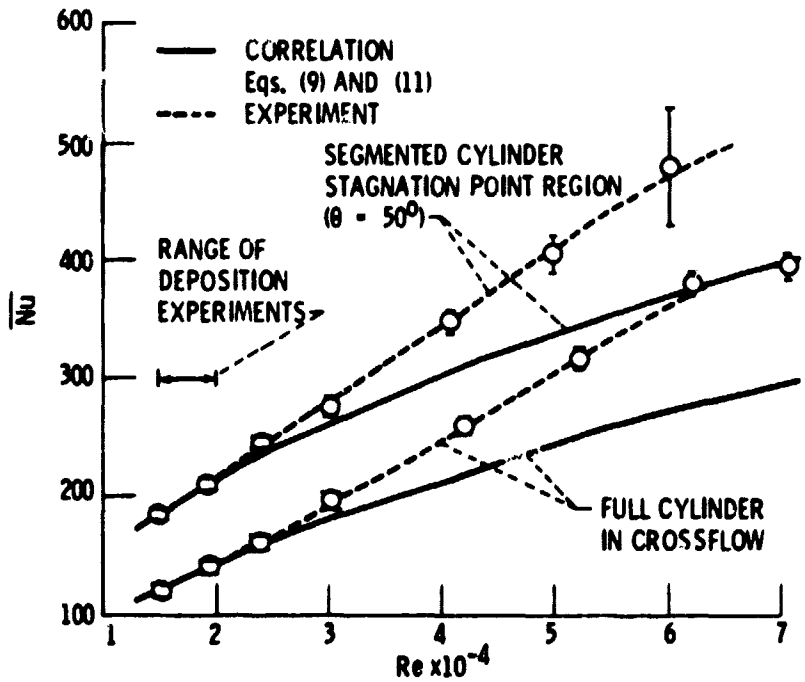

Figure 6. - Full and segmented cylinder mass transfer Nusselt number as a function of Reynolds number (based on cylinder diameter).

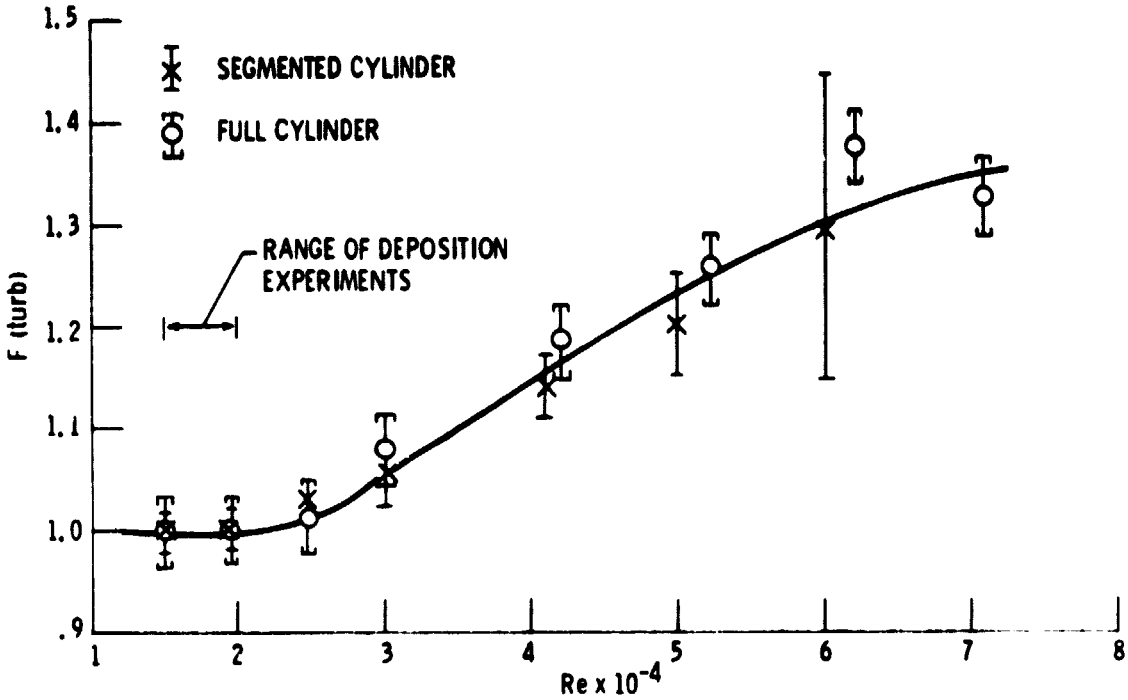

Figure 7. - Mainstream turbulence factor, F(turb), as a function of Reynolds number (based on cylinder diameter) for the burner rig experiments.

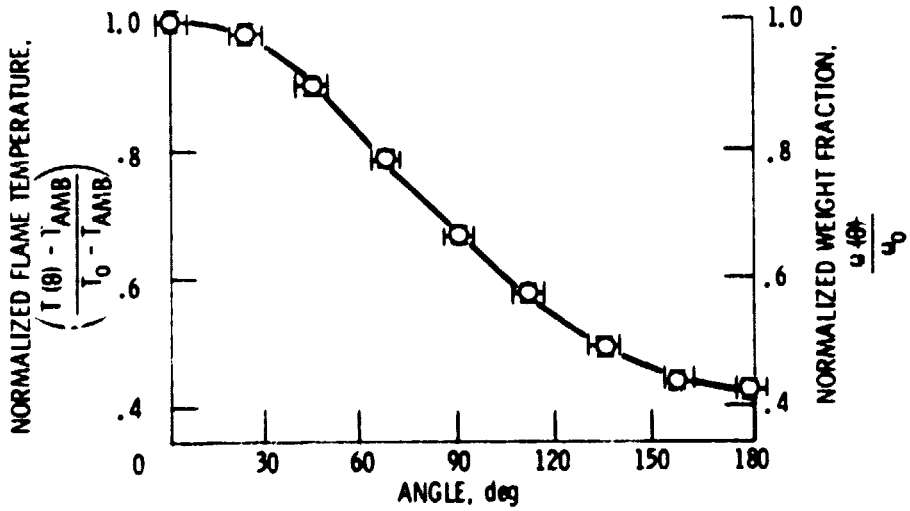

Figure 8. - Mainstream temperature and species mass fraction distribution around the collector as obtained from surface temperature measurements of collectors made of different materials for the range of operation of burner rig.

ORIGINAL PAGE IS
OF POOR QUALITY

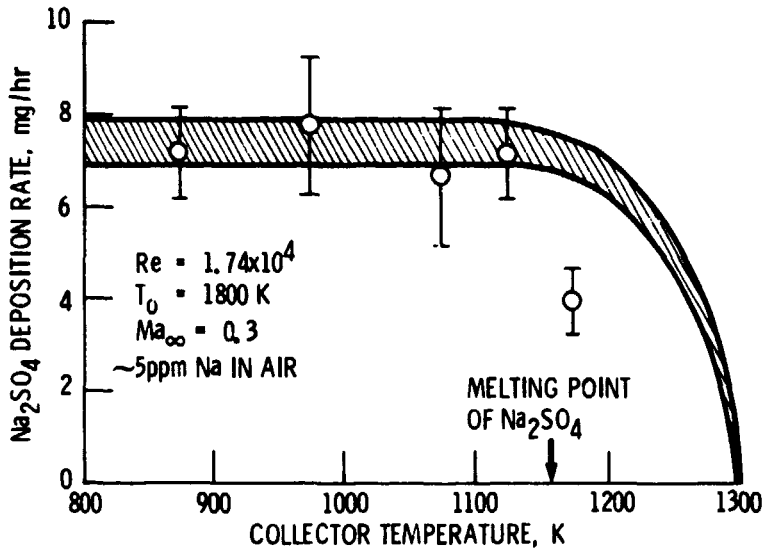

Figure 9. - Comparison of predicted and experimental sodium sulfate deposition rates for burner rigs.

1. Report No.	2. Government Accession No.	3. Recipient's Catalog No.
NASA TM-87176		

4. Title and Subtitle	5. Report Date
Determination of Convective Diffusion Heat/Mass Transfer Rates to Burner Rig Test Targets Comparable in Size to Cross-Stream Jet Diameter	6. Performing Organization Code 533-04-12
7. Author(s) Süleyman A. Gökoğlu and Gilbert J. Santoro	8. Performing Organization Report No. E-2722
	10. Work Unit No.
9. Performing Organization Name and Address National Aeronautics and Space Administration Lewis Research Center Cleveland, Ohio 44135	11. Contract or Grant No.
	13. Type of Report and Period Covered Technical Memorandum
12. Sponsoring Agency Name and Address National Aeronautics and Space Administration Washington, D.C. 20546	14. Sponsoring Agency Code

15. Supplementary Notes

Süleyman A. Gökoğlu, Case Western Reserve University, Dept. of Mechanical and Aerospace Engineering, Cleveland, Ohio 44106 and NASA Resident Research Associate; Gilbert J. Santoro, NASA Lewis Research Center, Cleveland, Ohio 44135.
Prepared for the 31st International Gas Turbine Conference sponsored by the American Society of Mechanical Engineers, Dusseldorf, Germany, June 8-12, 1986.

16. Abstract

Two sets of experiments have been performed to be able to predict the convective diffusion heat/mass transfer rates to a cylindrical target whose height and diameter are comparable to, but less than, the diameter of the circular cross-stream jet, thereby simulating the same geometric configuration as a typical burner rig test specimen located in the cross-stream of the combustor exit nozzle. The first set exploits the naphthalene sublimation technique to determine the heat/mass transfer coefficient under isothermal conditions for various flow rates (Reynolds numbers). The second set, conducted at various combustion temperatures and Reynolds numbers, utilizes the temperature variation along the surface of the above-mentioned target under steady-state conditions to estimate the effect of cooling (dilution) due to the entrainment of stagnant room temperature air. The experimental information obtained is used to predict high temperature, high velocity corrosive salt vapor deposition rates in burner rigs on collectors that are geometrically the same. The agreement with preliminary data obtained from Na_2SO_4 vapor deposition experiments is found to be excellent.

17. Key Words (Suggested by Author(s))	18. Distribution Statement
Deposition; Mass transfer; Cylinder in crossflow; Burner rigs; Corrosion; Heat transfer; Entrainment	Unclassified - unlimited STAR Category 34

19. Security Classif. (of this report)	20. Security Classif. (of this page)	21. No. of pages	22. Price*
Unclassified	Unclassified		

*For sale by the National Technical Information Service, Springfield, Virginia 22161